



저작자표시-비영리-변경금지 2.0 대한민국

이용자는 아래의 조건을 따르는 경우에 한하여 자유롭게

- 이 저작물을 복제, 배포, 전송, 전시, 공연 및 방송할 수 있습니다.

다음과 같은 조건을 따라야 합니다:



저작자표시. 귀하는 원저작자를 표시하여야 합니다.



비영리. 귀하는 이 저작물을 영리 목적으로 이용할 수 없습니다.



변경금지. 귀하는 이 저작물을 개작, 변형 또는 가공할 수 없습니다.

- 귀하는, 이 저작물의 재이용이나 배포의 경우, 이 저작물에 적용된 이용허락조건을 명확하게 나타내어야 합니다.
- 저작권자로부터 별도의 허가를 받으면 이러한 조건들은 적용되지 않습니다.

저작권법에 따른 이용자의 권리는 위의 내용에 의하여 영향을 받지 않습니다.

이것은 [이용허락규약\(Legal Code\)](#)을 이해하기 쉽게 요약한 것입니다.

[Disclaimer](#)

공학석사 학위논문

Reconstruction of 3D Human Lymphatic Vessel Network for Oncoimmunological Research

면역 항암 연구를 위한

삼차원 인간 림프관 체외 모델 개발

2021 년 2 월

서울대학교 대학원

공과대학 협동과정 바이오엔지니어링 전공

강 하 빈

면역 항암 연구를 위한
삼차원 인간 림프관
체외 모델 개발




Reconstruction of 3D Human
Lymphatic Vessel Network for
Oncoimmunological Research

지도교수 전 누 리

이 논문을 공학석사 학위논문으로 제출함
2020 년 12 월

서울대학교 대학원
공과대학 협동과정 바이오엔지니어링 전공
강 하 빈

강하빈의 공학석사 학위논문을 인준함
2021 년 1 월

위 원 장	도 준 상	(인) 
부위원장	전 누 리	(인) 
위 원	신 용 대	(인) 

Abstract

The lymphatic vessel (LV) plays an important role in cancer biology as a major route for tumor metastasis. Whereas, recent oncoimmunological approaches have focused its role in immune surveillance. In response to the emerging topics of lymphatic vascular biology, physiologically relevant human cell-based *in vitro* model is in high demand. This study introduces a 3D *in vitro* model of human LV within tumor immune microenvironment (TIME) using an injection-molded plastic array culture platform (Lymph-IMPACT). Through spontaneous capillary flow-driven patterning of 3D cellular hydrogel and optimized cellular composition, the platform enables robust and reproducible formation of self-organized LV *in vitro*. This co-culture model recapitulates cancer cell type-dependent morphogenesis of LV *in vitro*. Moreover, the robustness of the model enables high-content analysis on the effect of anti-VEGFR3 drug depending on the existence of blood vessels or different types of cancer cells. By virtue of high perfusability of 3D lumenized *in vitro* LV, a trans-endothelial migration of cytotoxic primary lymphocytes, which is one of the critical processes in anti-tumor immunology, is recapitulated within reconstructed melanoma TIME. From drug testing to cellular migration assays using the high-throughput platform, the Lymph-IMPACT demonstrates its powerful potential to be applied on investigating lymphatic-related strategies for cancer therapeutics.

Keyword : lymphatic vessel, tumor immune microenvironment, organ-on-a-chip, high-throughput platform, 3D *in vitro* model, lymphocyte migration assay

Student Number : 2019-22507

Table of Contents

Chapter 1. Introduction.....	1
Chapter 2. Result and Discussion	5
2.1. Reconstruction of 3D LV Network on High-Throughput Platform.....	5
2.2. High-Content Profiling of 3D LV Network Co-Cultured with Multiple Types of Cancer Cells	8
2.3. Anti-VEGFR3 Drug Treatment Analysis on Tumor LV Network Neighboring with Blood Vessel Network	12
2.4. Trans-Lympahtic Endothelial Migration of Cytotoxic Lymphocyte in Perfusable 3D LV Network.....	18
Chapter 3. Experimental Section	23
3.1. Fabrication of the Injection-Molded Plastic Array 3D Culture (IMPACT) Platform	23
3.2. Cell Culture	23
3.3. Hydrogel and Cell Patterning for 3D LV Network Formation	25
3.4. Drug Treatment	26
3.5. Immunocytochemistry	26
3.6. Cytotoxic Natural Killer (NK) Cell Cancer Killing Assay with Live Imaging	27
3.7. Cytokine Analysis	28
3.8. Imaging and Statistical Image Analysis on Vessel Morphology	29
3.9. Statistical Analysis	30
Chapter 4. Conclusion.....	31
Bibliography	33

Supporting Information.....	42
Abstract in Korean	46

Chapter 1. Introduction

The lymphatic vessel (LV) plays an important role in the maintenance of tissue fluid homeostasis, fat metabolism and immunity.^[1, 2, 3, 4] LVs connect lymphoid organs and coordinate trafficking of antigen and immune cells.^[2] While LVs have been known to complement tumor metastasis,^[3] recent oncoimmunological approaches suggest that LVs can serve as a route for immune surveillance.^[2, 4] Relating to this debatable role of LV in cancer therapeutics, the development of appropriate model for lymphatic studies is in increasing demand.

Compared to the long history of blood vascular research, the study of LVs has lagged behind due to the lack of specific markers of lymphatic endothelial cells (LEC) until late 1990s.^[5] Since then, the basic function and development of LVs have been actively investigated using transgenic mouse models mainly focused on the role of biochemical and genetic cues.^[6] Otherwise, the increased attention on human pathologies involving the malfunction of LVs such as lymphedema or lymphatic metastasis requires adequate human cell-based model which recapitulates multiple pathological microenvironmental cues. Conventional *in vitro* models of LEC ranging from 2D dish culture to 3D morphogenesis culture (e.g., tubulogenesis assay and lymphatic ring assay)^[7] have extended the scope of lymphatic vascular research, but still show limitations in reconstituting physiologically relevant functions derived from 3D lumen structures or the surrounding multi-cellular microenvironment.

In the last decade, advances in biotechnology have led to the development of 3D microphysiological systems (MPS), including the microfluidic-based organ-on-a-chip platform. The system has contributed to both fields of vascular and cancer biology by providing functional assays designed to solve specific biological questions.^[8] Moreover, advanced blood vascularized tumor models are now being practically used in cancer therapeutic studies.^[9] Despite the importance of LV and lymphangiogenesis on cancer progression, till date only a few 3D MPS models of LV are reported.^[10] Kim et al.^[11] was the first to introduce lymphangiogenesis-on-a-chip with 3D lumenized lymphatic sprouts reconstituted via synergic effect of biomechanical stimuli and pro-lymphangiogenic biochemical factors. The model showed high reproducibility suitable for screening the effect of diverse growth factors or drugs on lymphangiogenesis. LV models paired with blood vessel (BV) were also reported to emphasize the cooperative role of different types of endothelium partially sharing similar biomolecular mechanisms and vascular functions.^[12] Recently, David J. Beebe and colleagues have developed the human LV model by applying human LECs on artificial cylindrical wall made by the lumen rod inside a 3D matrix.^[13] Through functionalized assays such as the measurement of vascular permeability and drainage property, the changes of LV barrier function depending on various microenvironmental cues could be studied using the model. The same group also reported a study of the crosstalk between LV and breast cancer using their previously developed organotypic LV model.^[14] These recent cases collectively demonstrate that LV MPS

could function as a powerful tool for delineating specific function or pathology of lymphatic system in the tumor microenvironment (TME). However, in terms of application on cancer therapeutics, there is a need for LV models in its current state to improve in its robustness and reproducibility. Since the biomolecular mechanisms of LV were mentioned as the next target for anti-cancer drug,^[15] high-content and high-throughput model will be required for screening diverse drug candidates. Moreover, as various types of immune cells trafficking LV to reach the tumor site is the major issue of emerging cancer immunotherapy,^[4] an efficient model to test multiple combinations of crosstalk among diverse types of cells in tumor immune microenvironment (TIME) should be developed.

In this study, we report a 3D *in vitro* model of human LV within TIME using an injection molded plastic array culture platform (Lymph-IMPACT). The 3D cellular hydrogel is robustly loaded on the microfluidic channel by the spontaneous capillary flow-driven patterning method, then LV network is reconstructed inside the channel by self-organization of LEC with the help of neighboring stromal cells and cocktail of pro-lymphangiogenic factors. The robustness in the reconstitution of 3D *in vitro* tumor lymphatic microenvironment using Lymph-IMPACT leads to its application in high-content assays for assessing the effect of diverse cancer types on LV morphogenesis. Moreover, based on reconstituted TIME in co-existence of blood vessel network, we investigated the response of VEGFR3 inhibitor on multiple co-culture conditions. Finally, by virtue of the high perfusability of

the 3D lumenized LV network generated in Lymph-IMPACT, we were able to conduct 3D trans-endothelial migration assay using cytotoxic lymphocyte, primary natural killer (NK) cells. Collectively, our 3D *in vitro* LV network with high physiological relevance to native LVs in TIME, may contribute as a powerful research tool in the field of lymphatic system and especially in oncoimmunological therapeutics.

Chapter 2. Result and Discussion

2.1. Reconstruction of 3D LV Network on High-Throughput Platform

To recapitulate biological interactions and cellular responses at the site of LV in the TME (Figure 1a), a robust reconstitution of 3D LV network on high-throughput platform was preceded. This high-throughput injection-molded chip consists of 28 wells, and the size of each well is equal to two wells of a commercial 384-well plate (Figure 1b i). Each well consists of a cell loading channel at the center and two media reservoirs (Figure 1bii). Human LECs and fibroblasts were mixed with fibrin hydrogel, a commonly used scaffold material for successful *in vitro* 3D vascular formation^[12b, 16], then loaded on the center channel. Since LEC alone could not generate 3D LV network, fibroblasts were applied as a major source of pro-angiogenic or pro-lymphangiogenic factors as previously described in a number of studies in vascular engineering.^[11, 17] The ratio of LECs and fibroblasts in the mixture of cellular hydrogel was optimized to 2 : 1 (Figure S1), which resulted in the generation of highly lumenized vessels evenly dispersed at the center channel of the chip. With a single mixture of cellular hydrogel, a maximum of 28 samples with high reproducibility could be generated in a minute by virtue of the open microfluidic chip design, which is optimized for spontaneous capillary flow-based patterning, as described in our previous works.^[18] To generate highly perfusable network having its lumen opened intact, LECs were attached to each side of the gel wall to generate a

monolayer of lymphatic endothelium on both sides of the 3D patterned hydrogel (Figure 1biii). The culture medium contained a cocktail of pro-lymphangiogenic factors as previously described in the work of Kim et al.^[11] Although the components of the cocktail remains the same as the original protocol, we halved the concentration of each factor since the original concentration resulted in hyper-proliferation of LEC (Figure S2). This protocol resulted in formation of a fully lumenized and reproducible LV network within the center channel on the each well in 3–4 days of culture (Figure 1biii, 1c, and 1e). LV phenotype was verified by immunofluorescence staining of Podoplanin (PDPN), lymphatic vessel endothelial receptor 1 (LYVE1), and Prospero homeobox protein 1 (PROX1) (Figure 1d). In addition, vessel maturity was confirmed by immunostaining basal lamina protein, collagen IV, and the junctional protein, VE-cadherin.^[19]

To test the perfusability of 3D vessel network, fluorescein isothiocyanate-dextran (FITC-Dextran) (70 kDa) solution was introduced into the vessel network through the one its reservoirs, and the vessel lumen was immediately filled with fluorescence solution (Figure 1f). For additional verification on perfusability, micro-beads (2 μ m; Fluoro-Max, Thermo Scientific) were flown within the LV network (Figure S3). The characteristic of *in vitro* LV network with high perfusability enables its application in studying trans-endothelial cellular migration, which is the critical step in cancer metastasis or anti-tumoral immune activity. Furthermore, the cellular self-organization method to generate this highly perfusable LV

network will contribute to the robustness of related studies.

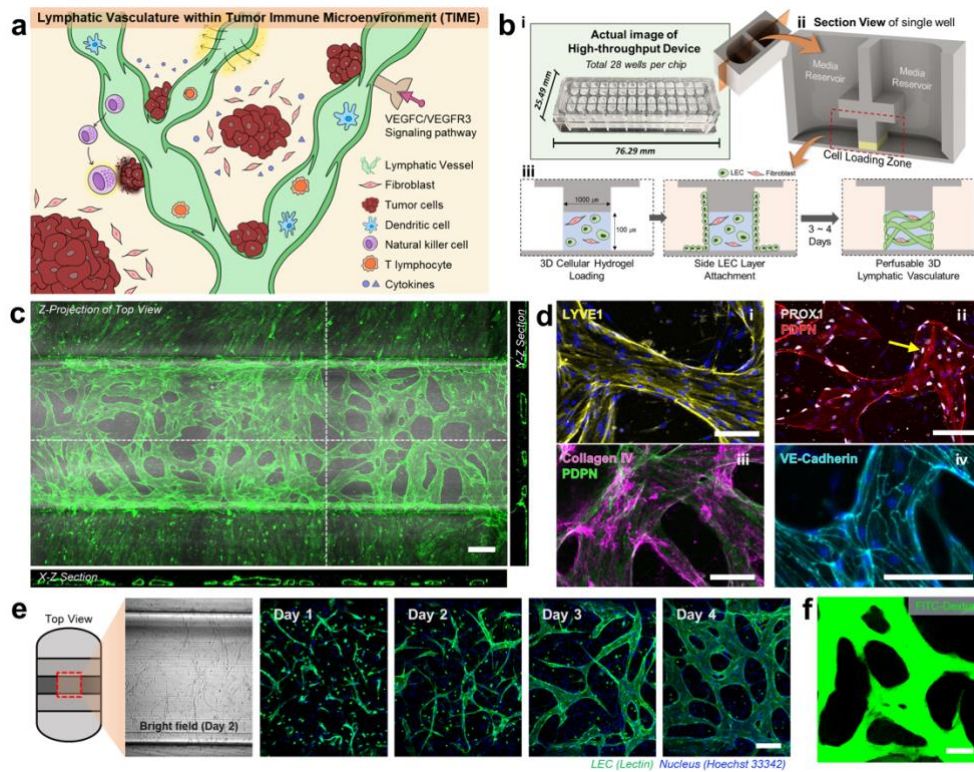


Figure 1. Reconstruction of 3D perfusable human LV network on high-throughput microfluidic platform. (a) Schematic overview of various biological phenomena at the site of lymphatic vessels (LV). (b) (i) Design of injection-molded high-throughput device. (ii) Section view of a single well, representing channel configuration. (iii) Stepwise protocol of 3D cellular hydrogel and side LEC attachment for reconstituting 3D human LV network *in vitro*. (c) Confocal image of the whole LV network in a chip immunostained with anti-PDPN (green) merged with DIC image in top view with z-projection. Cross-section views (x-z section and y-z section) shows fully lumenized LV networks. Scale bar = 200 μm . (d) Z-projected confocal image of lymphatic specific marker LYVE1 (yellow, i), PROX1 (white, indicated as yellow arrow, ii), and PDPN (red). Confocal image of basal lamina protein collagen IV (magenta, iii) covering LV (green, iii). Confocal image of adherens junction VE-Cadherin (cyan, iv). Scale bar = 100 μm . (e) Z-projected confocal images of day by day formation of LV network labeled with lectin staining. Red square in top view chip schematic indicates region of interest while imaging. Different samples loaded on same day with same culture condition are fixed in each day. Scale bar = 200 μm . (f) FITC-Dextran 70kDa flown within LV network to verify perfusability of the vessel network. Scale bar = 100 μm .

2.2. High-Content Profiling of 3D LV Network Co-Cultured with Multiple Types of Cancer Cells

Studies estimated that 80% of solid tumor metastases occur through LVs, while the rest occur through the BVs.^[20] Therefore, several therapeutic strategies to target molecular mechanisms governing tumor lymphangiogenesis or lymphatic function have been suggested. In compliance with the rising significance of regulating LVs in cancer therapeutics, we adopted our robust 3D human LV *in vitro* model to establish a 3D lymphatic TME with various types of cancer cells. Our Lymph-IMPACT platform, which enables high-throughput sample production, was used to assess the morphological phenotypes of 3D LV in each cancer co-culture environment. Six types of cancer cells, SK-MEL-2 (human melanoma), MDA-MB-231 (human breast cancer), U-87MG (human glioblastoma), HepG2 (human hepatocellular carcinoma), A549 (adenocarcinomic human alveolar basal epithelial cells), and SW480 (human colorectal carcinoma), were co-cultured with HDLECs and fibroblasts in the center channel of the chip as a mixture with 3D fibrin hydrogel. These cancer cell lines were selected to represent each type of cancer in which the LV highly contributes to their progression and metastasis (Supplementary Table 1).^[4b, 21] All conditions resulted in successful formation of robust LV networks on day 3 (Figure 2a). Confocal images of LVs of each co-culture conditions showed noticeable differences in morphology, mainly in vessel density and diameter.

To investigate the structural properties of the LV network quantitatively,

two widely used parameters were adopted. Vessel area relates with vessel density and thickness, and the number of vessel junctions serve as a parameter for vessel interconnectivity.^[22] Results indicated that LV co-cultured with MDA-MB-231 and U-87MG showed smaller area of z-projected vessel network compared to ones without cancer (Figure 2b). When measured in detail, the area of vessel network was 1.16-fold lower in the MDA-MB-231 co-culture conditions compared to that with no cancer condition, and the area of vessel network was 1.09-fold higher in the A549 co-culture conditions compared to that with no cancer condition. The number of vascular junctions was also measured to quantify the difference in the degree of vessel connectivity among co-culture conditions (Figure 2c). Co-culture conditions, which formed thick vessels with large vessel area measurement, resulted in smaller number of vascular junctions. In particular, LV network co-cultured with A549 showed 1.18-fold reduction in the number of vascular junctions compared to that with no cancer condition. Through the robustness of the platform enabling high-content profiling of multiple experiment conditions, we assessed a total of seven conditions of 3D tissue and TME in a single set of experiment. This demonstrates the capacity of this platform to capture heterogenic phenotype of LVs co-cultured with various cancer cell types on the established 3D tissue microenvironment in a high-throughput manner.

Taking a deeper look into the TME reconstructed in this platform, a sample co-cultured with SK-MEL-2, a melanoma cell line, was imaged in higher resolution (Figure 2d). SK-MEL-2 cells stained with CellTrace™ Far

Red (red) in advance of chip loading were located in the extravascular region proximal to the vascular surface as cell clusters, which are indicated with a yellow arrow in Figure 2d. Nuclei (blue) positioning on the extravascular region which are not detected as cancer cells indicate normal fibroblasts. Although all types of cancers used in this assay do not have direct interaction with fibroblasts *in vivo*, fibroblasts were co-cultured since cancer alone could not form 3D LV network. This is a limitation of the model as fibroblasts may cause undefined complex cellular interactions. In further applications of this model, SK-MEL-2 co-culture condition was selected as a representative cancer microenvironment, since there are a number of cases in melanoma studies related to lymphatics or cancer immunotherapy.^[4b, 15b]

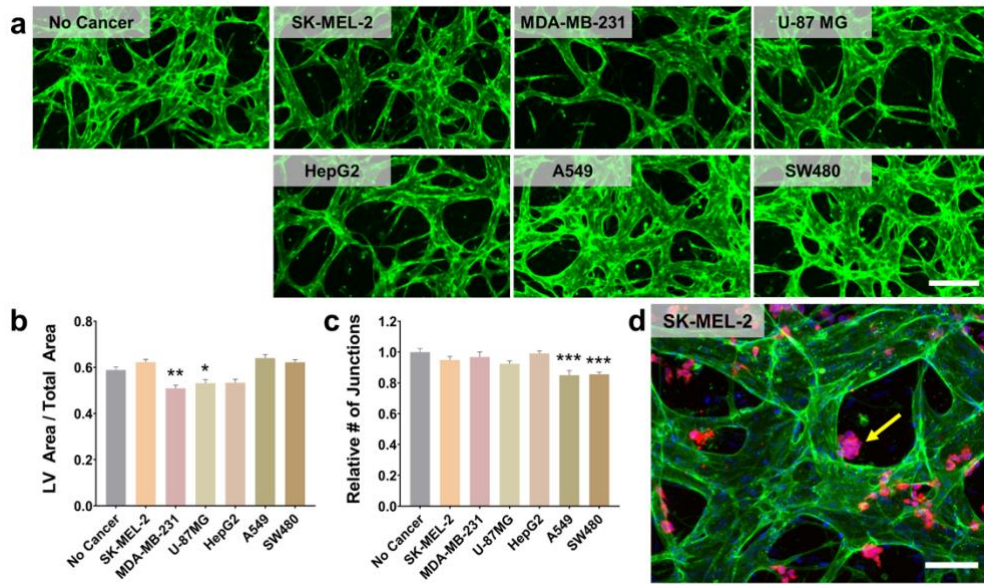


Figure 2. High-content profiling of LV network co-cultured with multiple types of cancer cells. (a) Representative z-projected confocal images of LV network on day 3 (labeled with lectin staining, green) co-cultured with six different types of cancer cells. Scale bar = 200 μ m. (b), (c) Quantitative analysis on LV area and the number of vascular junctions in each experiment condition. (* $p < 0.05$; ** $p < 0.01$; *** $p < 0.001$, One-way ANOVA with subsequent Tukey's multiple comparisons post-test, $N = 14$ for no cancer samples and $N = 7$ for each cancer co-culture condition) (d) Z-projected confocal image of LV network within melanoma (SK-MEL-2) microenvironment in higher magnification. LV is stained using lectin (green), SK-MEL-2 cells are stained with CellTraceTM Far Red (red) in advance of chip loading, and nucleus is stained using Hoechst 33342 (blue). The cluster of cancer cells is indicated with yellow arrow. Scale bar = 100 μ m.

2.3. Anti-VEGFR3 Drug Treatment Analysis on Tumor LV Network Neighboring with Blood Vessel Network

The regulation of VEGF-C/VEGFR3 signaling received attention as a novel anti-tumoral strategy for suppressing tumor lymphangiogenesis which could lead to metastasis.^[23] Previous studies reported that VEGFR3 inhibitors such as Cediranib (pan-VEGFR tyrosine kinase inhibitor) or SAR131675 (selective VEGFR3 tyrosine kinase inhibitor) possess the potential to improve the anti-tumoral effect when combined with traditional anti-VEGF/VEGFR2 therapies, but the clear effect and mechanism remain unsolved.^[15a] Moreover, it has been reported that the suppression of VEGFR3 could diminish tumor angiogenesis or blood vessel formation as well^[24] since VEGFR3 is up-regulated exceptionally in the blood microvasculature on tumor site.^[15b] We could also find a series of references mentioning crosstalk over mechanisms between angiogenesis and lymphangiogenesis.^[12c, 20, 25] Therefore, we designed an anti-VEGFR3 drug test assay on 3D human tumor LV alone or in co-existence with blood vessel network. While the platform has the potential to test diverse reagents regulating angiogenesis, or lymphangiogenesis, or both in high-content manner, we focused on a single inhibitor in this study to discover how the co-existence of LV and BV could affect the sensitivity of the drug compared to the sole-type culture of the endothelium *in vitro*. Among various VEGFR3 tyrosine kinase inhibitors, we selected SAR131675 due to its high selectivity on VEGFR3 despite VEGFR2.^[23a]

The robust modeling of *in vitro* 3D LV network was followed by SAR131675 treatment in concentration of 1 μ M and 10 μ M, 2 days after cell loading with media change. Control condition samples were prepared with or without dimethyl sulfoxide (DMSO). The area of both two vessel networks on day 3 was quantified individually through 3D confocal fluorescent imaging (Figure 3a). Both LV and BV showed a decrease in area when treated with SAR131675 compared to control samples. Apparently, the decrease in LV area was more dramatic compared to that of BV (Figure 3b). Specifically, in the case of MDA-MB-231 TME, the ratio of 10 μ M SAR131675 treated mono-cultured LV area to that of DMSO control was 0.251, while the same ratio on mono-cultured BV area was 0.600.

We also focused on how neighboring BV could influence LV in drug response. For intuitive comparison on drug response to LV among co-culture conditions, we presented relative area of LV in Figure 3c. Since the control LV area measurements are inconsistent among co-culture conditions, we normalized all area measurements to the average of each corresponding DMSO control measurements. Mono-cultured LV with or without cancer showed more sensitivity to 10 μ M SAR131675 treatment compared to LV co-cultured with BV. For example, in the case of TME with MDA-MB-231, the ratio of average LV area with drug treatment over DMSO control was 0.251 for the mono-cultured LV and 0.563 for the LV co-cultured with BV. The presented data imply that LV networking, especially in TME, could be affected by neighboring BV in terms of the VEGFR3 signaling pathway. A similar result was reported in recent *in vitro*

study by Osaki et al.,^[12c] which showed that SAR131675 inhibited lymphangiogenesis of LEC more strongly without the HUVEC compared to the co-culture conditions.

In addition, we analyzed the change in cancer cell population in response to the treatment of VEGFR3 inhibitor (Figure S4). On day 3, a day after 10 μ M SAR131675 treatment on day 2, the number of cancer cells were quantified to represent the effect of the drug on cancer cell proliferation. As a result, the number of cancer cells in the inhibitor-treated groups were 0.83-fold and 0.85-fold lower than that of DMSO control groups for SK-MEL-2 and MDA-MB-231 co-culture, respectively (Figure S4b and S4d). Though the results were statistically significant for both co-culture conditions, it did not show dramatic decrease in the number of cancer cells. We expect that the longer treatment of the inhibitor will result in a greater decrease in the number of cancer cells. Our result showing the decrease in the cancer cell population due to the VEGFR3 inhibitor treatment correlates with the previous studies that demonstrate VEGFR3 is also expressed in tumors including human breast cancer, not only in LVs. Moreover, these studies have discussed that VEGF-C/VEGFR3 signaling regulates tumor growth and metastasis.^[26] This result indicates that the platform is eligible for testing the efficacy of the drug on cancer cells as well as on vessel network, simultaneously.

The experimental set introduced in this study for testing drug efficacy consists of a total 36 different conditions (four drug treatment conditions, including control, DMSO control, SAR131674 1 μ M and 10 μ M, and nine

distinct co-culture conditions). By virtue of the robustness of Lymph-IMPACT using high-throughput platform, these multiple conditions were tested in a single experimental set at the same time while requiring a relatively small number of cells. Moreover, co-network of blood and lymphatic vessel which highly resembles the 3D structure of *in vivo* tissue^[1d, 27] could be reconstructed in high-throughput manner (Figure 3d). This demonstrates the capacity of the model to efficiently assess numerous drug candidates on physiologically relevant TME, which responds to the increasing demand of high-throughput platform in the field of cancer therapeutics.^[28]

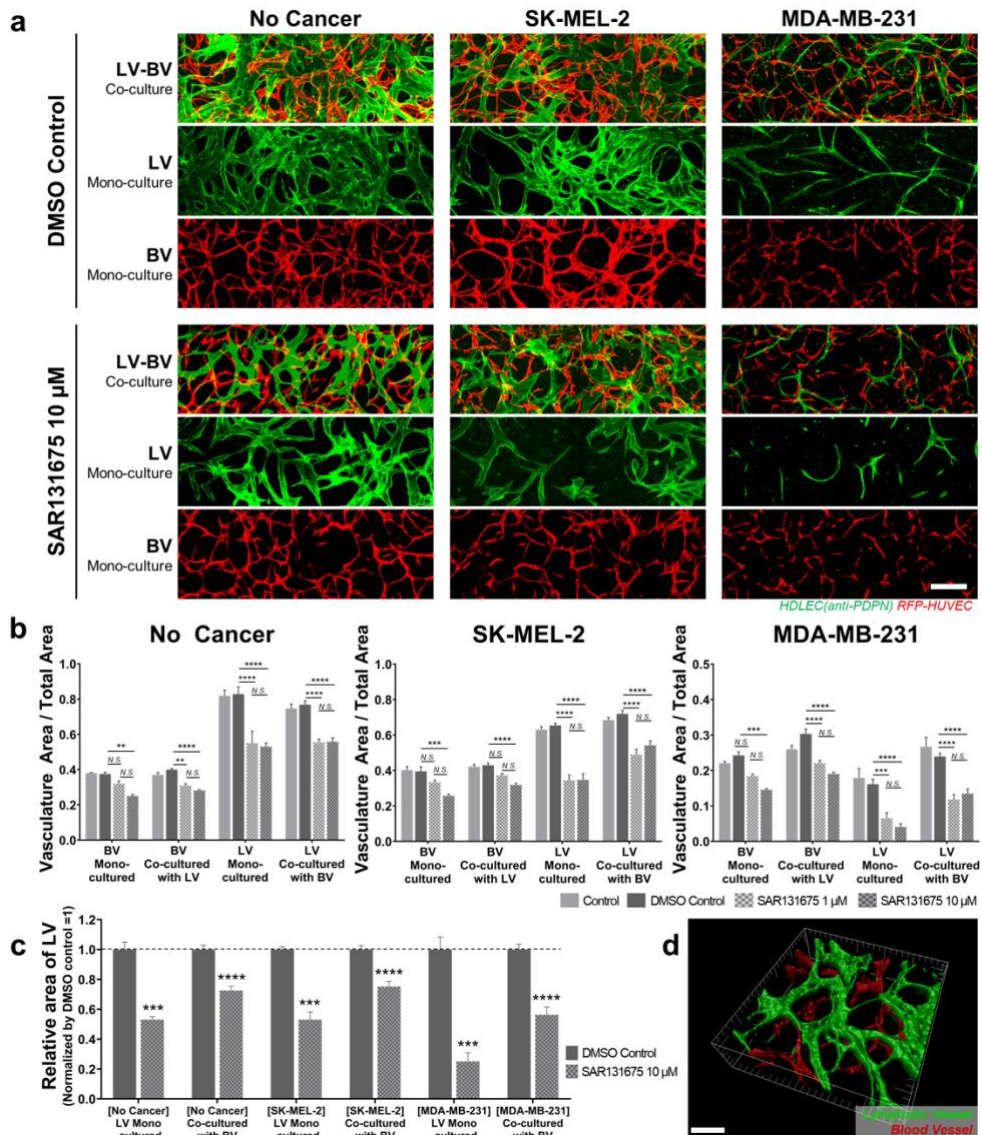


Figure 3. High-content screening of anti-VEGFR3 drug response on lymphatic and blood vessel network. Total 36 conditions were tested according to types of cultured vessel network (lymphatic, blood, or both), types of cancer cell co-cultured (no cancer, SK-MEL-2, or MDA-MB-231), and treatment conditions of the anti-lymphangiogenic drug (control, DMSO control, SAR131675 1 μ M, or SAR131675 10 μ M). Control media or media with corresponding concentration of the drug were supplied through media reservoir on Day 2. (a) Representative z-projected confocal images of vessel networks fixed on Day 4. Scale bar = 300 μ m. (b) Quantification of vessel areas in each condition. (c) Relative LV vessel area of anti-VEGFR3 treated samples over that of DMSO control samples in each co-culture condition. DMSO control values of each condition were normalized to 1.

(* $p < 0.05$; ** $p < 0.01$; *** $p < 0.001$, **** $p < 0.0001$. Two-way ANOVA with subsequent Tukey's multiple comparisons post-test for analysis in Figure 3b, and unpaired t-test for analysis in Figure 3c. N = 3 or 4 for each LV or BV mono-culture condition, and N = 5 to 8 for each LV-BV co-culture condition.) (d) 3D reconstruction of the representative confocal image of LV-BV co-culture condition with SAR131675 10 μ M treatment. Scale bar = 100 μ m.

2.4. Trans-Lymphatic Endothelial Migration of Cytotoxic Lymphocyte in Perfusable 3D LV Network

Since immunotherapy is the emerging tide of cancer therapeutics, researchers have shown great interest in the systemic circulation of diverse immune cells, referred to as “the cancer-immunity cycle”.^[29] Even though a large portion of immune cells in our body including lymphocytes exists in LVs, much is still unknown about the interactions between the LECs and immune cells in lymphatic circulation.^[4a, 30] Therefore, we developed a trans-endothelial migration assay of lymphocyte using our highly perfusable 3D human dermal LV model within a melanoma microenvironment. Since the NK cells are experimentally easily accessible lymphocytes compared with T cells and also known to exist in the lymphatic circulation,^[31] we have demonstrated our lymphocyte migration assay with NK cells. Moreover, NK cells are gaining attention as a potent tool for clinical cancer immunotherapy, especially for melanoma due to their main role in early anti-tumor immune response and its activation following adaptive immune responses against melanoma.^[4b, 32]

As previously described, highly perfusable 3D LV using human dermal LEC with or without melanoma cell line, SK-MEL-2, was generated for 3 days inside the microfluidic chip. On day 4, lymphocyte migration assay was conducted by introducing primary NK cells for live tracking. 1 h after applying NK cells in the intraluminal region of the LV network, live imaging was conducted for 7 h with 15 min interval (Figure 4a). The primary NK cells were tracked by pre-treated CellTraceTM Far Red fluorescence

(indicated as red in Figure 4b). Dead cells including melanoma cells attacked by cytotoxic NK cells were recognized with SytoxTM staining (indicated as blue in Figure 4b) during live imaging. Although the entire SytoxTM fluorescence could not specifically indicate the death of melanoma cells, which is a limitation of the method, we assumed ones that showed CellTraceTM CFSE fluorescence (indicated as white in Figure 4b) at the initial phase of live imaging as melanoma cells since the dye was uptaken only by melanoma cells in advance to chip loading. Interestingly, melanoma cells attached intimately on the outer surface of LV were attacked by NK cells in 1 h (indicated with yellow arrows in Figure 4b). Alternatively, aggregates of melanoma cells distant from LV embedded on 3D fibrin hydrogel were attacked by actively migrating NK cells around 6 h after the start of live imaging (indicated with pink arrows in Figure 4b). This clearly indicates that the infiltration of lymphocytes toward tumor cells depends on the surrounding 3D microenvironment and distance between the tumor and vessel network. Our result is consistent with previous studies on how the 3D matrix within the TME can influence the transport of anti-tumor immune cells toward solid tumor sites.^[33] For the live imaging of samples without melanoma cancer cells (Supplementary Video 6), NK cells showed active trans-endothelial migration through the LV network, whereas SytoxTM fluorescence indicating cell death was less detected compared to the samples with cancer cells.

In addition to the 3D matrix, chemokine composition in the lymphatic microenvironment is another dominant factor directing the trans-endothelial

trafficking of leucocytes in inflammation or cancer pathology.^[31a] Therefore, we investigated the difference in biochemical components between 3D lymphatic microenvironment with or without melanoma cells using the human cytokine array kit. On day 4, just before the introduction of NK cells into 3D tumor lymphatic microenvironment, supernatants from 7 samples were collected and pooled as $n = 1$ for the cytokine analysis. For each condition, $n = 3$ analyses (collected from 21 samples) resulted in quantitative detection of four different types of cytokine (IL-4, IL-5, CXCL1, and CXCL10) (Figure 4c and Figure S5). Among them, the expression of IL-4 is likely elevated and that of IL-5 significantly increased in melanoma co-cultured samples compared to those without cancer (Figure 4d). This result is consistent with previous studies on skin cancer showing elevated secretion levels of IL-5 and IL-4.^[34] One of these studies have emphasized IL-4 as an important cytokine in the suppression of melanoma development mediated by activated NK cells.^[34d] On the other hand, some studies have drawn attention to these cytokines for inducing pro-tumorigenic responses.^[34b, 34c] Although the expression of CXCL1 or CXCL10 was not significantly dependent on the existence of melanoma cells, these cytokines were widely studied in relation to cancer progression, immune homeostasis, and lymphatics. CXCL1 expressed in melanoma microenvironment is reported to play a major role in tumorigenesis, angiogenesis, and metastasis.^[35] Another study discussed the role of CXCL10 in immune activation including immune cell migration, differentiation, and activation.^[36] Moreover, these two CXC chemokines were reported to be expressed by

LECs and promote cancer metastasis toward the lymph node.^[37]

The global measurement of biochemical cues in our reconstructed 3D *in vitro* microenvironment partially mimics the *in vivo* cytokine components which plays an important role in tumorigenesis, cancer metastasis, and immune cell migration. Thus, the model reveals its potential for studying the effect of various biomolecular pathways on trans-lymphatic endothelial migration of lymphocytes or even cancers. Recent studies have demonstrated the interaction between cancer and immune cells *in vitro*, however, most studies do not include vessel network which is a key component of TIME.^[38] Considering this, Lymph-IMPACT suggests a more physiologically relevant model by being able to capture the complex cellular interactions under the existence of LV network.

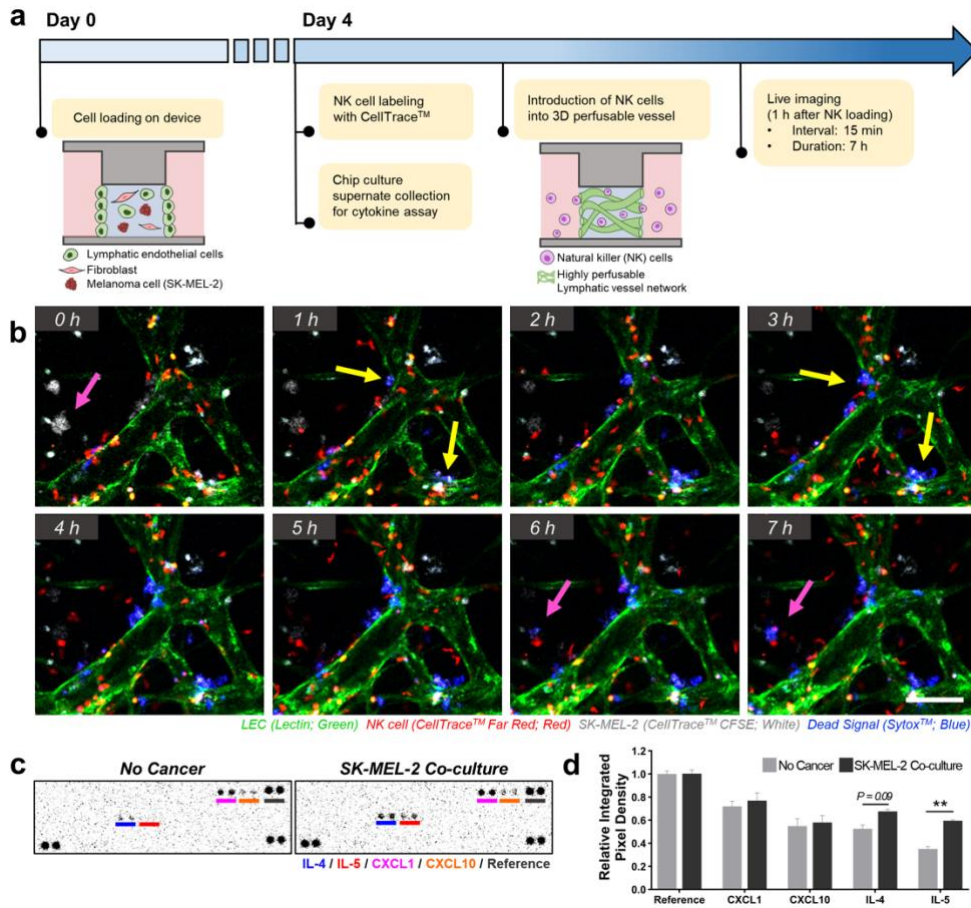


Figure 4. Trans-lymphatic endothelial migration of cytotoxic lymphocyte in perfusable 3D LV network. (a) Schematic illustration of experimental timeline from initial cell loading to live cell imaging. (b) 1 h interval images of 3D confocal live cell imaging on primary NK cell migrating LV network co-cultured with SK-MEL-2. (Live imaging was started 1 h after NK cell loading and maintained for 7 h, in 15 min interval.) Pink arrows indicate the aggregates of melanoma cells distant from LV. Yellow arrows indicate the aggregates of melanoma cells attached intimately on the outer surface of LV. Scale bar = 100 μ m. (c) Result of global cytokine analysis on supernate collected from *in vitro* lymphatic microenvironment with or without SK-MEL-2. (d) Relative integrated pixel density of detectable cytokines: CXCL1, CXCL10, IL-4, and IL-5. All values are normalized by average of integrated pixel density on reference spot as 1. (** $p < 0.01$. Two-way ANOVA with subsequent Tukey's multiple comparisons post-test for analysis. Each supernate sample for cytokine analysis was acquired from 7 chips. Total 3 pooled samples for each co-culture condition was applied for cytokine analysis.)

Chapter 3. Experimental Section

3.1. Fabrication of the Injection–Molded Plastic Array 3D Culture (IMPACT) Platform

Device was made with polystyrene (PS) by injection molding performed at R&D Factory (Korea). Manufacturing of the aluminum alloy mold core was done through machining and polishing. Injection was performed at a clamping force of 130 ton, maximum injection pressure of 55 bar, cycle time of 15 seconds, and nozzle temperature of 220°C. The resulting PS substrate was bonded with a pressure sensitive adhesive-coated polycarbonate film which works as a chip bottom.

3.2. Cell Culture

Human dermal lymphatic endothelial cells (HDLECs; Lonza, Swiss) were cultured in microvascular endothelial growth medium 2 (EGM-2 MV) with pro-lymphangiogenic cocktail added to facilitate LV formation. The cocktail consists of vascular endothelial growth factor-A (VEGF-A, R&D Systems), VEGF-C (R&D Systems), basic fibroblast growth factor (bFGF, Invitrogen), sphingosine-1-phosphate (S1P, Sigma), and recombinant human endocan (ESM-1, R&D Systems).^[11] The factors were added to culture medium at final concentrations of 25 ng mL⁻¹ for VEGF-A and bFGF, 50 ng mL⁻¹ for VEGF-C and ESM-1, and 0.5 μM for S1P. HDLECs of passages 5 to 6 were used for experiments. RFP expressing human umbilical vein endothelial cells (RFP-HUVECs; Angioproteomie, USA) were cultured in endothelial

growth medium 2 (EGM-2; Lonza) and passage 4 were used for experiments. Normal human lung fibroblasts (Lonza) were cultured in fibroblast growth medium 2 (FGM-2; Lonza) and passages 6 to 7 were used for experiments. SK-MEL-2 (gifted from Dr. Junsang Doh in Department of Materials Science and Engineering, Seoul National University, Korea), GFP-tagged MDA-MB-231, GFP-tagged U-87 MG and GFP-tagged HepG2 (both gifted from Dr. Kyung Sun Kang in College of Veterinary Medicine, Seoul National University, Korea), GFP-tagged A549 (gifted from Dr. Jangho Kim in College of Agriculture and Life Sciences, Seoul National University, Korea), and GFP-tagged SW480 (Angioproteomie, USA) were cultured in RPMI-1640 (Gibco, USA) supplemented with 10% fetal bovine serum (HyClone, USA) and 1% penicillin-streptomycin (Gibco, USA). All cells were incubated at 37°C in 5 % CO₂ for 3 days prior to loading on device, and were detached from culture dishes using 0.25% trypsin-EDTA (HyClone, USA). Expanded NK cells were generated as described in previous work by SH Kweon et al.,^[39] from peripheral blood mononuclear cells (PBMCs) by co-culture with irradiated K562-OX40L feeder cells in complete RPMI1640 (RPMI 1640 supplemented with 10% heat-inactivated FBS, 100 U mL⁻¹ penicillin, 100 µg mL⁻¹ streptomycin and 4 mmol L⁻¹ L-glutamine) plus 10 IU mL⁻¹ rhIL-2 in 24-well tissue culture plate. For vigorous proliferation, IL-2 concentration was increased to 100 U mL⁻¹ and 5 ng mL⁻¹ soluble IL-15 was added to the medium from day 7. Expanded NK cells from day 14-21 were cryopreserved and used for NK cell killing assay with Live Imaging when needed.

3.3. Hydrogel and Cell Patterning for 3D LV Network Formation

Chips were plasma surface treated for 3 minutes at 70 W before experiments to induce surface hydrophilicity (Femto Science, Korea). Fluid patterning within the device was done first on the center channel and then the side channels (if needed). Center channels were patterned with a fluid mixture composed of 25 μL of HDLECs, 12.5 μL of fibroblasts, and 12.5 μL of 10 mg mL^{-1} fibrinogen solution (Sigma, USA). Final concentrations of HDLECs and fibroblasts were $4 \times 10^6 \text{ cells mL}^{-1}$ and $2 \times 10^6 \text{ cells mL}^{-1}$, respectively. In culture conditions including cancer cells, 5 μL of cancer cells were added to the 50 μL fluid mixture resulting in final concentration of $0.3 \times 10^6 \text{ cells mL}^{-1}$. In case of blood and lymphatic vessel co-culture for drug testing experiments, RFP-HUVECs, HDLECs, fibroblasts, and fibrinogen solution was mixed in same volume 12.5 μL to generate final concentration $8 \times 10^6 \text{ cells mL}^{-1}$, $2 \times 10^6 \text{ cells mL}^{-1}$, $2 \times 10^6 \text{ cells mL}^{-1}$, and 2.5 mg mL^{-1} , respectively. This optimized concentration resulted in LV network formation having similar total area with mono-cultured LV network generated by the aforementioned protocol. 0.9 μL of the final mixture was patterned and captured in each center channel as fluid injection along the edge of each well spontaneously filled the center channel due to spontaneous capillary flow. The primed hydrogel mixture was then allowed to crosslink for 10 minutes before further patterning or medium supply. The side channel was patterned with 3 μL of HDLEC suspension in concentration of $3 \times 10^6 \text{ cells mL}^{-1}$, and the device was tilted upright for 20 minutes in the

incubator to let the cells evenly pile up on the created hydrogel interface. The opposite side channel was consecutively patterned in the same manner. After fluid patterning processes, media reservoir was filled with 200 μL of medium per well.

3.4. Drug Treatment

A selective VEGFR-3 inhibitor, SAR131675 (Selleck, USA), was dissolved in DMSO according to the manufacturer's instructions. The inhibitor was then diluted into two different concentrations (1 and 10 μM) with culture medium and introduced into the media reservoir two days after initial cell loading on device. Two types of control medium were set considering the addition of DMSO; control medium (EGM-2 MV with cocktail) and DMSO control medium (control medium with equal amount of DMSO added to prepare 10 μM VEGFR-3 inhibitor).

3.5. Immunocytochemistry

Cultured tissues in the device were fixed with 4% (w/v) paraformaldehyde (Biosesang, Korea) for 20 minutes, and then were permeabilized with 0.2% Triton X-100 (Sigma) for 20 minutes followed by treatment with 3% BSA (Millipore, USA) for 40 minutes. Rabbit polyclonal anti-human lymphatic vessel endothelial receptor 1 (LYVE1) (1:100; Reliatech; 102-PA50), Prospero homeobox protein 1 (PROX1) (1:100; Reliatech; 102-PA32), and Collagen IV (1:100; Abcam; ab6586) were treated for 2 to 3 days as primary antibodies non-conjugated with

fluorescent markers. These primary antibody stained samples were subsequently incubated with Alexa Fluor 568 goat anti-rabbit immunoglobulin G (IgG) (1:1000; Inbitrogen; A11036) as secondary antibody overnight. Alexa Fluor 488/594/647-conjugated anti-human Podoplanin (PDPN) (1:200; Biolegend; 337005/337018/337007), Alexa Fluor 488-conjugated mouse anti-human VE-Cadherin (1:200; eBioscience; 53-1448-42), and Alex Fluor 594-conjugated mouse anti-human α -Smooth Muscle Actin (α -SMA) (1:200; R&D systems; IC1420T) were treated for 2 to 3 days. Two types of lectin, fluorescein-conjugated Ulex Europaeus Agglutinin 1 (1:1000; Vector; FL-1061) and DyLight 594-conjugated Ulex Europaeus Agglutinin 1 (1:1000; Vector; DL-1067), were used for staining LEC which have been established as a marker for both human blood and lymphatic endothelial cells.^[40] Alexa Fluor 488-conjugated phalloidin and Hoechst 33342 (1:1000; Molecular Probes) were treated overnight for staining F-actin and DNA, respectively. All samples were washed with PBS and stored at 4°C until imaging.

3.6. Cytotoxic Natural Killer (NK) Cell Cancer Killing Assay with Live Imaging

Live imaging was performed with Nikon Ti2-E inverted microscope (Nikon Eclipse Ti, Japan) on day 4 from initial cell seeding. SK-MEL-2 cells and NK cells were labeled with either CellTraceTM Far Red Cell Proliferation Kit (Thermo Fisher, C34572) or CellTraceTM CFSE Cell Proliferation Kit (Thermo Fisher, C34570) by incubating the cells in serum

free RPMI-1640 with 1 μM and 5 μM of each reagent respectively for 30 min. To label dead cells during live imaging, SytoxTM Blue Dead Cell Stain (Thermo Fisher, C34857) was used in 1:1000 dilution in culture medium. Prior to introducing NK cells, HDLECs, fibroblasts, and SK-MEL-2 cells were seeded within fibrin hydrogel and cultured for 3 days, allowing reconstitution of 3D tissue containing perfusable LVs with co-existing SK-MEL-2 cells. On day 3, NK cells (1×10^6 cells mL^{-1}) suspended in culture medium were loaded on the device through both top and bottom media reservoirs. While 15 μL and 30 μL of culture medium containing NK cells were injected in top and bottom media reservoirs, respectively, the device was tilted upright for 15 minutes in the direction where the bottom reservoir is displaced higher, and then was inverted in the opposite direction for 15 minutes. This was done to ensure even positioning of NK cells within the cultured tissue and formed lymphatic tube. Finally, LV culture medium including IL-2 and IL-15 was added to the media reservoirs. Live imaging was then initiated in the time interval of 15 minutes for total 8 hours.

3.7. Cytokine Analysis

Live Composition of global cytokine in tumor lymphatic microenvironment was quantitatively analyzed using Proteome Profiler Human Cytokine Array Kit (ARY005B, R&D Systems). On day 4, just before introducing NK into the 3D tumor lymphatic microenvironment, supernatants from 7 samples were collected and pooled as $n = 1$ for cytokine array analysis with instruction provided by the manufacturer. $N = 3$ (pooled from

total 21 samples) were analyzed for each condition with or without cancer cell co-culture, respectively.

3.8. Imaging and Statistical Image Analysis on Vessel Morphology

Imaging was performed with Nikon Ti2-E inverted microscope (Nikon Eclipse Ti, Japan) with microscope software NIS elements (Nikon). Used objective was Plan Apo λ 10 \times (Numerical Aperture: 0.45, Nikon). Acquired confocal images were processed with Fiji (<http://fiji.sc.>), an open access software. 3D confocal images were stacked into 2D images by z-projection in max intensity, and were cropped to defined region of interest. For the measurement of vessel area, equal threshold value was applied to each image and was converted to binary mask. Then, pixel area of each binary mask image was measured directly with Fiji. In addition, the number of vascular junctions was measured by utilizing Angiogenesis Analyzer, a free software plugin for ImageJ and Fiji.^[41] The original z-projected confocal images were denoised and contrast enhanced using Fiji. All images from a single set of experiment were applied with identical setting using macro. The denoised and contrast enhanced images were converted to RGB type in advance, then directly applied to the software. Setting for analysis was ‘Analyze HUVEC Fluo’, and no other setting was altered. Angiogenesis Analyzer produced a quantified measurement for each image in diverse parameters including vessel junction. For the measurement of the number of cancer cells, equal threshold value was applied to each fluorescent z-

projected image of cancer and was converted to binary mask. Then, the 'Watershed' function in Fiji was applied to masked image to dissect the clustered cancer cells into individual cells. Finally, the cells were automatically counted by the 'Analyze Particles' in Fiji. For 3D reconstruction of the confocal image in Figure 3d or Supplementary Video 6, Imaris (Bitplane) was used.

3.9. Statistical Analysis

To obtain statistical comparisons of the measurements, unpaired two-tailed Student's t-test or two-way ANOVA with subsequent Tukey's multiple comparison post-test was performed using GraphPad Prism 9 software. The p-value thresholds for statistical significance were set and represented in the graphs as *p < 0.05; **p < 0.01; ***p < 0.001; ****p < 0.0001; *N.S.*, not significant. All error bars in the graphs present standard error of the mean (SEM). The sample size (N) for each statistical analysis is described in detail on each figure caption.

Chapter 4. Conclusion

In this study, we presented a reproducible and robust *in vitro* model of 3D human LV using a high-throughput platform, termed Lymph-IMPACT. With emerging topics in cancer biology regarding the role of LV in TIME, we reconstituted the 3D tumor LV network showing distinct morphogenic phenotypes determined by different cancer types. The robustness of this platform enabled the high-content analysis of drug response in nine different co-culture conditions at a single experimental set. The high perfusability of 3D lumenized LV was applied to the trans-endothelial migration assay of immune cells, which is the critical step of anti-tumor immune activity. Not being limited to NK cells, diverse types of immune cells can further be applied to the platform for studying its role in the lymphatic system as well as its interaction with LV. Furthermore, distinct from previous organotypic *in vitro* models of LV, the LV network in our model was generated as a self-organization method, which made sample generation extremely robust, as well as increased the physiological relevancy of the model by enhancing cellular interaction between the LV and its surrounding TIME.

Though our study focused on the role of LV in cancer therapeutics including oncoimmunological approach, the model can be applied as a human cell-based 3D *in vitro* model to study diverse pathologies involving the LV such as skin inflammation and lymphedema. Our model will provide a wide perspective to biomedical researchers mainly relying on transfected mouse

models to elucidate developmental or pathological mechanisms of the lymphatic system. Moreover, researchers working on pharmaceutical approaches to regulate lymphatic functions against cancers or lymphatic diseases could benefit from our high-throughput platform for robust and efficient screening of drug candidates. Taken together, our robust human LV model with highly perfusable 3D structure based on a high-throughput platform shows great potential to function as a powerful and efficient tool for lymphatic studies and development of novel therapeutics.

Bibliography

- [1] a) K. Alitalo, *Nature medicine* 2011, 17, 1371; b) K. Alitalo, T. Tammela, T. V. Petrova, *Nature* 2005, 438, 946; c) G. Oliver, *Nature Reviews Immunology* 2004, 4, 35; d) P. Saharinen, T. Tammela, M. J. Karkkainen, K. Alitalo, *Trends in Immunology* 2004, 25, 387.
- [2] G. J. Randolph, S. Ivanov, B. H. Zinselmeyer, J. P. Scallan, *Annual review of immunology* 2017, 35, 31.
- [3] a) Q. Ma, L. C. Dieterich, K. Ikenberg, S. B. Bachmann, J. Mangana, S. T. Proulx, V. C. Amann, M. P. Levesque, R. Dummer, P. Baluk, *Science advances* 2018, 4, eaat4758; b) N. E. Tobler, M. Detmar, *Journal of leukocyte biology* 2006, 80, 691; c) S. A. Stacker, M. G. Achen, L. Jussila, M. E. Baldwin, K. Alitalo, *Nature Reviews Cancer* 2002, 2, 573.
- [4] a) V. Angeli, P. K. Yeo, *Frontiers in Immunology* 2017, 8, 83; b) M. Fankhauser, M. A. Broggi, L. Potin, N. Bordry, L. Jeanbart, A. W. Lund, E. Da Costa, S. Hauert, M. Rincon-Restrepo, C. Tremblay, *Science translational medicine* 2017, 9.
- [5] a) M. Gröger, R. Loewe, W. Holnthoner, R. Embacher, M. Pillinger, G. S. Herron, K. Wolff, P. Petzelbauer, *The Journal of Immunology* 2004, 173, 7161; b) A. Kaipainen, J. Korhonen, T. Mustonen, V. Van Hinsbergh, G.-H. Fang, D. Dumont, M. Breitman, K. Alitalo, *Proceedings of the National Academy of Sciences* 1995, 92, 3566; c)

- J. T. Wigle, G. Oliver, *Cell* 1999, 98, 769; d) J. Wilting, M. Papoutsis, B. Christ, K. H. Nicolaides, C. S. von Kaisenberg, J. Borges, G. B. Stark, K. Alitalo, S. I. Tomarev, C. Niemeyer, *The FASEB Journal* 2002, 16, 1271.
- [6] a) R. Cao, S. Lim, H. Ji, Y. Zhang, Y. Yang, J. Honek, E.-M. Hedlund, Y. Cao, *Nature protocols* 2011, 6, 817; b) L. Yuan, D. Moyon, L. Pardanaud, C. Bréant, M. J. Karkkainen, K. Alitalo, A. Eichmann, *Development* 2002, 129, 4797.
- [7] F. Bruyère, A. Noël, *The FASEB Journal* 2010, 24, 8.
- [8] a) J. W. Andrejcsk, C. C. Hughes, *Current Opinion in Biomedical Engineering* 2018, 5, 74; b) S. Lee, J. Ko, D. Park, S.-R. Lee, M. Chung, Y. Lee, N. L. Jeon, *Lab on a Chip* 2018, 18, 2686; c) I. K. Zervantonakis, S. K. Hughes-Alford, J. L. Charest, J. S. Condeelis, F. B. Gertler, R. D. Kamm, *Proceedings of the National Academy of Sciences* 2012, 109, 13515; d) M. Chung, J. Ahn, K. Son, S. Kim, N. L. Jeon, *Advanced healthcare materials* 2017, 6, 1700196.
- [9] a) J. Ko, J. Ahn, S. Kim, Y. Lee, J. Lee, D. Park, N. L. Jeon, *Lab on a Chip* 2019, 19, 2822; b) S. Lee, J. Lim, J. Yu, J. Ahn, Y. Lee, N. L. Jeon, *Lab on a Chip* 2019, 19, 2071; c) A. Sobrino, D. T. Phan, R. Datta, X. Wang, S. J. Hachey, M. Romero-López, E. Gratton, A. P. Lee, S. C. George, C. C. Hughes, *Scientific reports* 2016, 6, 1; d) K. Haase, G. S. Offeddu, M. R. Gillrie, R. D. Kamm, *Advanced Functional Materials* 2020, 2002444; e) A. Boussommier-Calleja, Y. Atiyas, K. Haase, M. Headley, C. Lewis, R. Kamm, *Biomaterials* 2019, 198, 180;

- f) J. M. Ayuso, R. Truttschel, M. M. Gong, M. Humayun, M. Virumbrales-Munoz, R. Vitek, M. Felder, S. D. Gillies, P. Sondel, K. B. Wisinski, *OncoImmunology* 2019, 8, 1553477.
- [10] a) M. A. Luque-González, R. L. Reis, S. C. Kundu, D. Caballero, *Advanced Biosystems* 2020, 2000045; b) K. Margaris, R. A. Black, *Journal of the Royal Society Interface* 2012, 9, 601.
- [11] S. Kim, M. Chung, N. L. Jeon, *Biomaterials* 2016, 78, 115.
- [12] a) X. Cao, R. Ashfaq, F. Cheng, S. Maharjan, J. Li, G. Ying, S. Hassan, H. Xiao, K. Yue, Y. S. Zhang, *Advanced Functional Materials* 2019, 29, 1807173; b) L. Knezevic, M. Schaupper, S. Mühleder, K. Schimek, T. Hasenberg, U. Marx, E. Priglinger, H. Redl, W. Holnthoner, *Frontiers in Bioengineering and Biotechnology* 2017, 5, 25; c) T. Osaki, J. C. Serrano, R. D. Kamm, *Regenerative engineering and translational medicine* 2018, 4, 120; d) M. Sato, N. Sasaki, M. Ato, S. Hirakawa, K. Sato, K. Sato, *PloS one* 2015, 10, e0137301.
- [13] M. M. Gong, K. M. Lugo-Cintrón, B. R. White, S. C. Kerr, P. M. Harari, D. J. Beebe, *Biomaterials* 2019, 214, 119225.
- [14] J. M. Ayuso, M. M. Gong, M. C. Skala, P. M. Harari, D. J. Beebe, *Advanced Healthcare Materials* 2020, 9, 1900925.
- [15] a) I. Barry, *Nature Reviews Cancer* 2008, 8; b) T. V. Petrova, P. Bono, W. Holnthoner, J. Chesnes, B. Pytowski, H. Sihto, P. Laakkonen, P. Heikkilä, H. Joensuu, K. Alitalo, *Cancer cell* 2008, 13, 554; c) Y. Yonemura, S. Fushida, E. Bando, K. Kinoshita, K. Miwa, Y. Endo, K. Sugiyama, T. Partanen, H. Yamamoto, T. Sasaki, *European*

- Journal of cancer 2001, 37, 918.
- [16] a) A. Takei, Y. Tashiro, Y. Nakashima, K. Sueishi, *In Vitro Cellular & Developmental Biology–Animal* 1995, 31, 467; b) X. Feng, M. G. Tonnesen, S. A. Mousa, R. A. Clark, *International journal of cell biology* 2013, 2013; c) S. Kim, H. Lee, M. Chung, N. L. Jeon, *Lab on a Chip* 2013, 13, 1489.
 - [17] a) J. M. Sorrell, M. A. Baber, A. I. Caplan, *Cells Tissues Organs* 2007, 186, 157; b) A. C. Newman, M. N. Nakatsu, W. Chou, P. D. Gershon, C. C. Hughes, *Molecular biology of the cell* 2011, 22, 3791; c) L. A. Kunz-Schughart, J. A. Schroeder, M. Wondrak, F. van Rey, K. Lehle, F. Hofstaedter, D. N. Wheatley, *American Journal of Physiology–Cell Physiology* 2006, 290, C1385.
 - [18] Y. Lee, J. W. Choi, J. Yu, D. Park, J. Ha, K. Son, S. Lee, M. Chung, H.-Y. Kim, N. L. Jeon, *Lab on a Chip* 2018, 18, 2433.
 - [19] P. Baluk, J. Fuxe, H. Hashizume, T. Romano, E. Lashnits, S. Butz, D. Vestweber, M. Corada, C. Molendini, E. Dejana, *Journal of Experimental Medicine* 2007, 204, 2349.
 - [20] A. Alitalo, M. Detmar, *Oncogene* 2012, 31, 4499.
 - [21] a) S. A. Stacker, S. P. Williams, T. Karnezis, R. Shayan, S. B. Fox, M. G. Achen, *Nat Rev Cancer* 2014, 14, 159; b) C. Schietroma, F. Cianfarani, P. M. Lacal, T. Odorisio, A. Orecchia, J. Kanitakis, S. D'Atri, C. M. Failla, G. Zambruno, *Cancer* 2003, 98, 789; c) N. E. Tobler, M. Detmar, *J Leukoc Biol* 2006, 80, 691; d) Y. Nakamura, H. Yasuoka, M. Tsujimoto, S. Imabun, M. Nakahara, K. Nakao, M.

Nakamura, I. Mori, K. Kakudo, Breast cancer research and treatment 2005, 91, 125; e) M. Skobe, T. Hawighorst, D. G. Jackson, R. Prevo, L. Janes, P. Velasco, L. Riccardi, K. Alitalo, K. Claffey, M. Detmar, Nature medicine 2001, 7, 192; f) E. Song, T. Mao, H. Dong, L. S. B. Boisserand, S. Antila, M. Bosenberg, K. Alitalo, J. L. Thomas, A. Iwasaki, Nature 2020, 577, 689; g) A. Thelen, A. Scholz, C. Benckert, Z. von Marschall, M. Schroder, B. Wiedenmann, P. Neuhaus, S. Rosewicz, S. Jonas, Int J Cancer 2008, 122, 2471; h) V. Lukacs-Kornek, Front Immunol 2016, 7, 548; i) C. C. Schimanski, R. Bahre, I. Gockel, A. Muller, K. Frerichs, V. Horner, A. Teufel, N. Simiantonaki, S. Biesterfeld, T. Wehler, M. Schuler, T. Achenbach, T. Junginger, P. R. Galle, M. Moehler, Br J Cancer 2006, 95, 210; j) I. Takanami, Oncology reports 2006, 15, 437; k) F. Renyi-Vamos, J. Tovari, J. Fillinger, J. Timar, S. Paku, I. Kenessey, G. Ostoros, L. Agocs, I. Soltesz, B. Dome, Clin Cancer Res 2005, 11, 7344; l) K. Matsumoto, Y. Nakayama, Y. Inoue, N. Minagawa, T. Katsuki, K. Shibao, Y. Tsurudome, K. Hirata, N. Nagata, H. Itoh, Dis Colon Rectum 2007, 50, 308; m) R. S. Saad, L. Kordunsky, Y. L. Liu, K. L. Denning, H. A. Kandil, J. F. Silverman, Mod Pathol 2006, 19, 1317; n) A. Schoppmann, D. Tamandl, B. Herberger, F. Laengle, P. Birner, S. Geleff, T. Gruenberger, S. F. Schoppmann, Anticancer research 2011, 31, 4605.

- [22] B. A. Corliss, C. Mathews, R. Doty, G. Rohde, S. M. Peirce, Microcirculation 2019, 26, e12520.

- [23] a) A. Alam, I. Blanc, G. Gueguen-Dorbes, O. Duclos, J. Bonnin, P. Barron, M.-C. Laplace, G. Morin, F. Gaujarengues, F. Dol, *Molecular cancer therapeutics* 2012, 11, 1637; b) T. P. Padera, A. H. Kuo, T. Hoshida, S. Liao, J. Lobo, K. R. Kozak, D. Fukumura, R. K. Jain, *Molecular cancer therapeutics* 2008, 7, 2272.
- [24] T. Tammela, G. Zarkada, E. Wallgard, A. Murtomäki, S. Suchting, M. Wirzenius, M. Waltari, M. Hellström, T. Schomber, R. Peltonen, *Nature* 2008, 454, 656.
- [25] a) M. Lohela, M. Bry, T. Tammela, K. Alitalo, *Current opinion in cell biology* 2009, 21, 154; b) B. Regenfu, F. Bock, C. Cursiefen, *Current opinion in allergy and clinical immunology* 2012, 12, 548; c) F. Morfoisse, A. Noel, *The international journal of biochemistry & cell biology* 2019, 114, 105562.
- [26] a) M. L. Varney, R. K. Singh, *American journal of cancer research* 2015, 5, 616; b) J.-L. Su, C. Yen, P. Chen, S. Chuang, C. Hong, I. Kuo, H. Chen, M.-C. Hung, M. Kuo, *British journal of cancer* 2007, 96, 541.
- [27] J. Stachura, M. Wachowska, W. W. Kilarski, E. Güç, J. Golab, A. Muchowicz, *Oncoimmunology* 2016, 5, e1182278.
- [28] a) C. Probst, S. Schneider, P. Loskill, *Current Opinion in Biomedical Engineering* 2018, 6, 33; b) C. Beaurivage, E. Naumovska, Y. X. Chang, E. D. Elstak, A. Nicolas, H. Wouters, G. van Moolenbroek, H. L. Lanz, S. J. Trietsch, J. Joore, *International Journal of Molecular Sciences* 2019, 20, 5661.

- [29] a) D. S. Chen, I. Mellman, *Immunity* 2013, 39, 1; b) I. Mellman, G. Coukos, G. Dranoff, *Nature* 2011, 480, 480.
- [30] M. C. Hunter, A. Teijeira, C. Halin, *Frontiers in immunology* 2016, 7, 613.
- [31] a) D. G. Jackson, *Frontiers in immunology* 2019, 10, 471; b) H. Lund, P. Boysen, J. C. Hope, S. K. Sjurseth, A. K. Storset, *Frontiers in immunology* 2013, 4, 395; c) I. Melero, A. Rouzaut, G. T. Motz, G. Coukos, *Cancer discovery* 2014, 4, 522.
- [32] a) M. Granzin, A. Stojanovic, M. Miller, R. Childs, V. Huppert, A. Cerwenka, *Oncoimmunology* 2016, 5, e1219007; b) R. Tarazona, E. Duran, R. Solana, *Frontiers in immunology* 2016, 6, 649.
- [33] a) D. S. Foster, R. E. Jones, R. C. Ransom, M. T. Longaker, J. A. Norton, *JCI insight* 2018, 3; b) M. U. Mushtaq, A. Papadas, A. Pagenkopf, E. Flietner, Z. Morrow, S. G. Chaudhary, F. Asimakopoulos, *Journal for immunotherapy of cancer* 2018, 6, 65.
- [34] a) A. Birbrair, *Tumor Microenvironments in Organs: From the Brain to the Skin–Part A*, Springer, 2020; b) I. Elamin, R. D. Zecević, D. Vojvodić, L. Medenica, M. D. Pavlović, *Acta dermatovenerologica Alpina, Pannonica, et Adriatica* 2008, 17, 55; c) M. Georgouli, C. Herraiz, E. Crosas-Molist, B. Fanshawe, O. Maiques, A. Perdrix, P. Pandya, I. Rodriguez-Hernandez, K. M. Ilieva, G. Cantelli, *Cell* 2019, 176, 757; d) D. J. Son, Y. Y. Jung, M. H. Park, H. L. Lee, M. J. Song, H.-S. Yoo, D. Y. Hwang, S. B. Han, J. T. Hong, *Neoplasia* 2017, 19, 537.

- [35] a) P. Dhawan, A. Richmond, *Journal of leukocyte biology* 2002, 72, 9;
b) K. I. Amiri, A. Richmond, *Progress in nucleic acid research and molecular biology* 2003, 74, 1.
- [36] R. Tokunaga, W. Zhang, M. Naseem, A. Puccini, M. D. Berger, S. Soni, M. McSkane, H. Baba, H.-J. Lenz, *Cancer treatment reviews* 2018, 63, 40.
- [37] a) R. H. Farnsworth, T. Karnezis, S. J. Maciburko, S. N. Mueller, S. A. Stacker, *Frontiers in immunology* 2019, 10, 518; b) M. Haemmerle, T. Keller, G. Egger, H. Schachner, C. W. Steiner, D. Stokic, C. Neumayer, M. K. Brown, D. Kerjaschki, B. Hantusch, *Diabetes* 2013, 62, 2509; c) K. Kawada, H. Hosogi, M. Sonoshita, H. Sakashita, T. Manabe, Y. Shimahara, Y. Sakai, A. Takabayashi, M. Oshima, M. M. Taketo, *Oncogene* 2007, 26, 4679; d) K. Kawada, M. Sonoshita, H. Sakashita, A. Takabayashi, Y. Yamaoka, T. Manabe, K. Inaba, N. Minato, M. Oshima, M. M. Taketo, *Cancer research* 2004, 64, 4010; e) J. Xu, C. Zhang, Y. He, H. Wu, Z. Wang, W. Song, W. Li, W. He, S. Cai, W. Zhan, *International journal of cancer* 2012, 130, 787; f) Z. Wang, Z. Wang, G. Li, H. Wu, K. Sun, J. Chen, Y. Feng, C. Chen, S. Cai, J. Xu, *Cancer letters* 2017, 385, 28.
- [38] a) D. Park, K. Son, Y. Hwang, J. Ko, Y. Lee, J. Doh, N. L. Jeon, *Frontiers in immunology* 2019, 10, 1133; b) A. Pavesi, A. T. Tan, S. Koh, A. Chia, M. Colombo, E. Antonicchia, C. Miccolis, E. Ceccarello, G. Adriani, M. T. Raimondi, *JCI insight* 2017, 2; c) S. W. L. Lee, G. Adriani, E. Ceccarello, A. Pavesi, A. T. Tan, A. Bertoletti, R. D.

- Kamm, S. C. Wong, *Frontiers in immunology* 2018, 9, 416.
- [39] S. Kweon, M.-T. T. Phan, S. Chun, H. Yu, J. Kim, S. Kim, J. Lee, A. K. Ali, S.-H. Lee, S.-K. Kim, *Frontiers in immunology* 2019, 10, 879.
- [40] N. G. Ordóñez, T. Brooks, S. Thompson, J. G. Batsakis, *The American journal of surgical pathology* 1987, 11, 543.
- [41] S. Scalabrin, L. Toniutti, G. Di Gaspero, D. Scaglione, G. Magris, M. Vidotto, S. Pinosio, F. Cattonaro, F. Magni, I. Jurman, *Scientific reports* 2020, 10, 1.

Supporting Information

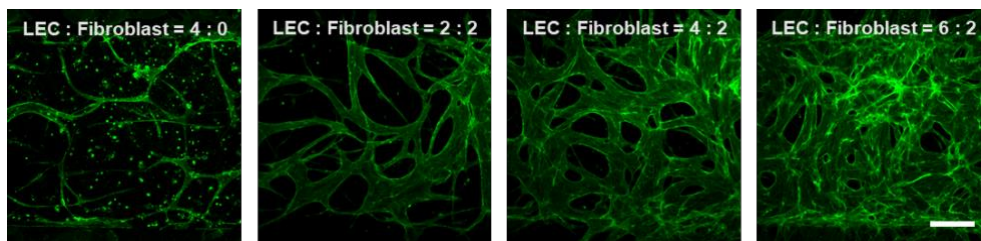


Figure S1. Optimizing the ratio of human dermal lymphatic endothelial cells and normal human lung fibroblasts. The ratio written on top of the images represent the ratio of concentration of lymphatic endothelial cells to fibroblasts (Unit: 10^6 cells mL^{-1}). Scale bar = 200 μm .

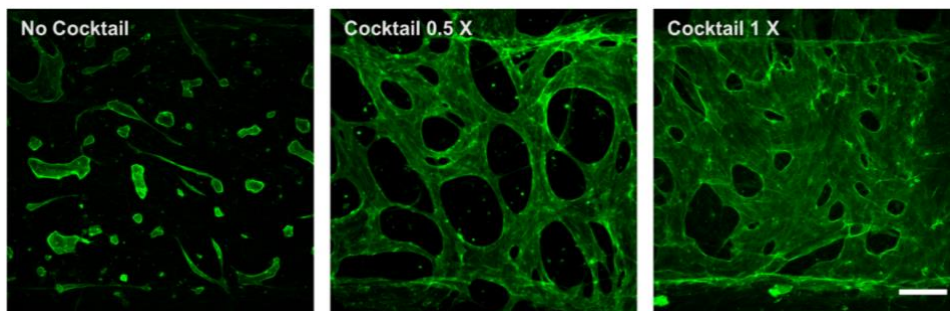


Figure S2. Optimizing the concentration of pro-lymphangiogenic factor cocktail added in culture media. The original protocol was previously introduced in the study of 3D microfluidic lymphangiogenesis model by Kim et al. (S. Kim, M. Chung, N. L. Jeon, Biomaterials 2016, 78, 115.), which resulted hyper-proliferation of LEC in lymphatic vascular network formation conducted in Lymph-IMPACT (right, Cocktail 1 X). The half of original concentration of the cocktail resulted optimized 3D lumenized network formation (right, Cocktail 0.5 X), whereas culture without the factors resulted no network formation of LECs (left, No Cocktail). All three images are z-projected confocal images immunostained with human anti-PDPN. Scale bar = 200 μm .

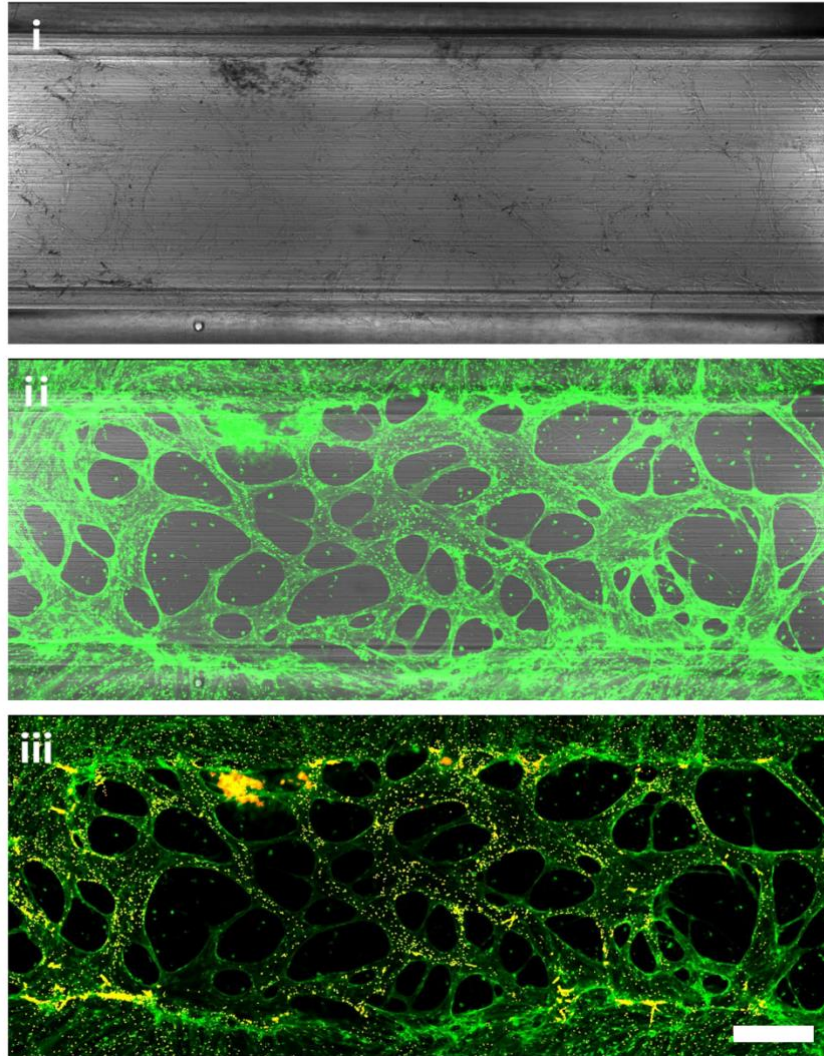


Figure S3. Verifying perfusability of 3D LV network in Lymph-IMPACT. Z-projected confocal image of the whole center channel of the chip. DIC image (i) is merged with confocal image of LV network stained with lectin (ii). Fluorescent micro-beads with 2 μm diameter (indicated as yellow in iii) is applied on the one end of the LV network and we could examine the flow of bead toward the other end of the network. Scale bar = 300 μm .

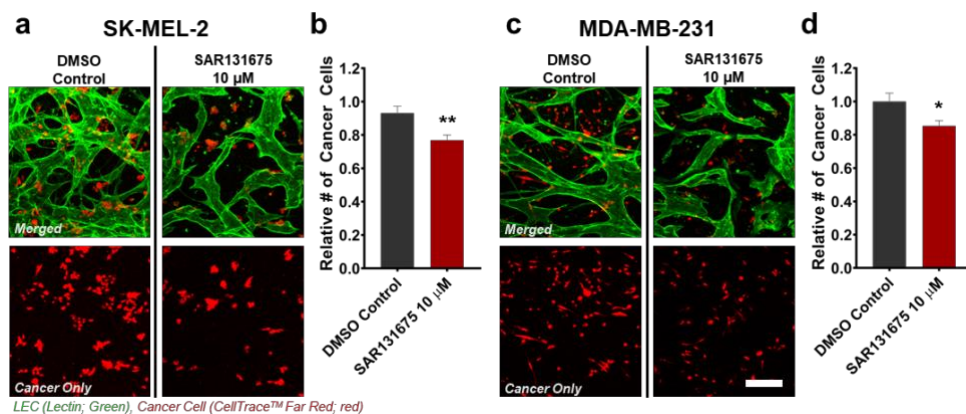


Figure S4. Analysis on the effect of SAR131675 treatment on cancer cells. (a) Representative z-stacked confocal images of LV network co-cultured with SK-MEL-2 in treatment of SAR131675 or DMSO as control. Below images represent cancer only, which is the same position of upper images. (b) Quantitative analysis in the number of cancer cells in each drug treatment condition in SK-MEL-2 coculture. (**p < 0.01. Unpaired two-tailed Student's t-test was performed to obtain statistical comparisons of analyzed values. N = 8 for DMSO control condition and N = 14 for SAR131675 treatment condition.) (c) Representative z-stacked confocal images of LV network co-cultured with MDA-MB-231 in treatment of SAR131675 or DMSO as control. Below images represent cancer only, which is the same position of upper images. (d) Quantitative analysis in the number of cancer cells in each drug treatment condition in MDA-MB-231 coculture. (*p < 0.05. Unpaired two-tailed Student's t-test was performed to obtain statistical comparisons of analyzed values. N = 14 for DMSO control condition and N = 14 for SAR131675 treatment condition.) Scale bar = 200 μm.

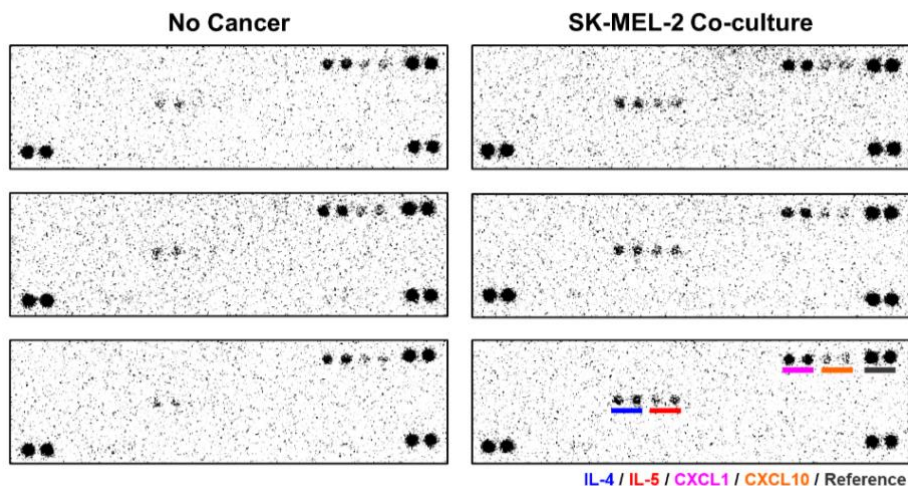


Figure S5. Result of X-ray imaged membranes in human cytokine array assay. Each membrane indicates cytokine detection in supernates collected from 7 samples cultured in same condition. Differentially detected dot pairs are indicated by different color lines.

Supplementary Table 1. Summary of the interplay between lymphatic vascular system and each type of cancer

Cancer Origin	Interplay Between Lymphatic Vascular System and Cancer	References
Skin	<ul style="list-style-type: none"> - Major route for lymphatic metastatic spread - High VEGF-C expression inducing tumor lymphangiogenesis - High VEGF-C expression promoting tumor immunosuppression - Lymphangiogenesis potentiating immunotherapy by promoting T cell infiltration 	Fankhauser <i>et al.</i> , 2017. ^[20] ; Tobler <i>et al.</i> , 2006. ^[21] ; Schietroma <i>et al.</i> , 2003. ^[21]
Breast	<ul style="list-style-type: none"> - Major route for lymphatic metastatic spread - High VEGF-C expression inducing tumor lymphangiogenesis - Lymphatic vessel density correlating lymph node metastasis and cancer prognosis 	Skobe <i>et al.</i> , 2001. ^[21] ; Nakamura <i>et al.</i> , 2005. ^[21]
Brain	<ul style="list-style-type: none"> - VEGF-C signaling promoting immune surveillance of glioblastoma (enhancing the priming of CD8T cells in the draining deep cervical lymph node) - VEGF-C signaling working synergistically with immune checkpoint blockade treatment 	Song <i>et al.</i> , 2020. ^[21]
Liver	<ul style="list-style-type: none"> - Correlation with the growth and metastasis potential of hepatocellular carcinoma - Lymphatic metastasis involved with CXCR4 signaling - Active dissemination of liver tumors expressing VEGF-C or VEGF-D 	Schimanski <i>et al.</i> , 2006. ^[21] ; L.-Kornek <i>et al.</i> , 2016. ^[21] ; Thelen <i>et al.</i> , 2008. ^[21]
Lung	<ul style="list-style-type: none"> - Novel and independent indicator for the lymph node metastasis in non-small lung cancer - Contribution on the growth of nonangiogenic non-small lung cancer 	R.-Vamos <i>et al.</i> , 2005. ^[21] ; Takamami <i>et al.</i> , 2006. ^[21]
Colon	<ul style="list-style-type: none"> - Lymphatic microvessel density as an independent prognostic factor of colorectal cancer (correlation with positive lymphatic vessel invasion) - Intratumoral VEGF-C expression associate with reduced patient survival 	Saad <i>et al.</i> , 2006. ^[21] ; Matsumoto <i>et al.</i> , 2006. ^[21] ; Schoppmann <i>et al.</i> , 2011. ^[21]

초록

림프관은 암 생물학 분야에서 암 전이의 통로 역할을 하는 것으로 널리 알려져 있다. 반면, 최근 면역 항암 분야에서 림프관은 면역 감시가 일어나는 곳으로 주목을 받으며, 이에 초점이 맞추어진 연구가 활발히 진행되고 있다. 이렇게 림프관에 관련한 연구 주제가 대두됨에 따라 생체 유사성이 높은 인간 세포 기반 체외 모델의 필요성이 커지고 있다. 위 연구에서는 플라스틱 세포배양 칩을 기반으로 삼차원 인간 림프관을 암-면역 미세환경 내에 구현한 체외 모델을 제시한다. 모세관 힘을 이용한 삼차원 세포-하이드로겔 패터닝과 최적화된 세포 구성으로 재현성 높은 자기 조직화 림프관을 고효율로 구현할 수 있다. 해당 모델을 활용하여 다양한 암세포의 공배양을 통해 사용된 암세포의 종류에 따라 달라지는 림프관의 형태를 재현하였다. 또한, 이 모델의 고효율성을 이용하여 혈관성장인자수용체-3 (anti-VEGFR3) 약물에 대한 반응을 혈관 및 다양한 암세포의 유무에 따라 분석하였다. 그리고 체외 삼차원 림프관의 높은 관류성을 활용하여 면역 항암 분야에서 주요한 과정 중 하나인 세포 독성 림프구의 경내피 이동을 흑색종 미세환경 내에서 재현하였다. 위 모델은 약물 스크리닝부터 세포의 이동 및 독성 활동 구현까지 가능하게 하는 고효율 플랫폼으로, 림프관에 관련한 암 치료법 연구에 강력한 도구로써 적용될 수 있음을 보인다.